Neutron diffraction, Mössbauer and magnetotransport study of Fe-substituted derivatives of $CaCu_3Mn_4O_{12}$ perovskite with colossal magnetoresistance

2007 J. Phys.: Condens. Matter 19 356209

(http://iopscience.iop.org/0953-8984/19/35/356209)

IOP PUBLISHING JOURNAL OF PHYSICS: CONDENSED MATTER

J. Phys.: Condens. Matter **19** (2007) 356209 (11pp) doi:10.1088/0953-8984/19/35/356209

Neutron diffraction, Mössbauer and magnetotransport study of Fe-substituted derivatives of $CaCu_3Mn_4O_{12}$ perovskite with colossal magnetoresistance

H Falcón[1], J Sánchez-Benítez[2], M J Martínez-Lope[1], J A Alonso[2,4], K Krezhov[3], I Spirov[3] and T Ruskov[3]

[1] Instituto de Ciencia de Materiales de Madrid, CSIC, Cantoblanco, E-28049 Madrid, Spain
[2] Centre for Science at Extreme Conditions and School of Engineering and Electronics, University of Edinburgh, King's Buildings, Mayfield Road, Edinburgh EH9 3JZ, UK
[3] Institute of Nuclear Research and Nuclear Energy, Bulgarian Academy of Sciences, 72 Tsarigradsko Chaussee Boulevard, Sofia, 1784, Bulgaria

E-mail: ja.alonso@icmm.csic.es

Received 22 March 2007, in final form 11 July 2007
Published 8 August 2007
Online at stacks.iop.org/JPhysCM/19/356209

Abstract

The effect of replacing Mn for Fe in the ferrimagnetic perovskite $CaCu_3Mn_4O_{12}$ has been studied in the series of nominal composition $CaCu_3(Mn_{4-x}Fe_x)O_{12}$ ($x = 0$, 0.5, 1.0). These materials have been prepared in polycrystalline form under moderate pressure conditions of 2 GPa, in the presence of $KClO_4$ as oxidizing agent. The $x = 1.0$ sample has been studied by neutron powder diffraction and Mössbauer spectroscopy to unravel some structural peculiarities. These oxides crystallize in the cubic space group $Im\bar{3}$ (No. 204) and contain Ca^{2+} and (Cu^{2+}, Mn^{3+}) at the A sublattice of the ABO_3 perovskite, arranged in a 1:3 ordered array. Neutron diffraction suggests that Mn^{4+} and Fe^{3+} occupy at random the octahedral B positions of the perovskite structure, whereas the Mössbauer study adds a singular feature: 89% of Fe^{3+} is, effectively, in an octahedral environment, whereas 11% of Fe^{3+} is located at square-planar positions together with Cu^{2+}. The materials have also been characterized by magnetic and magnetotransport measurements. All the samples are ferromagnetic and show a progressive decrease of T_C as the Fe contents increases. Also the saturation magnetization and Weiss temperatures diminish in the Fe-doped oxides, which suggest an increment of the antiferromagnetic interactions at the (Mn, Fe) octahedral sublattice. The magnetoresistance also decreases upon Fe doping, although a sharp low-field response is observed below T_C.

(Some figures in this article are in colour only in the electronic version)

[4] Author to whom any correspondence should be addressed.

0953-8984/07/356209+11$30.00

1. Introduction

There is an increasing demand of magnetoresistive materials to surpass their present abilities to be useful in the fast changing world of magnetoelectronic devices. At the root of all devices lie the bulk materials, on whose basic properties further progress may be made. Hence, the search for new materials showing colossal magnetoresistance (CMR) is of great importance. Moreover, before widespread practical applications can be made, an enhancement in their basic performance is required, mainly because the CMR response at low field and room temperature is negligible in the best known systems, such as the rare-earth manganese perovskites [1], or other more complex phases such as the $Tl_2Mn_2O_7$ pyrochlore or the iron double perovskites.

The complex perovskite $CaCu_3Mn_4O_{12}$ has also attracted some interest as a potential CMR material, given its ferromagnetic and half-semiconducting character [2–6]. This oxide was first reported by Chenavas *et al* [7], who prepared it under high-pressure conditions (7 GPa). This compound belongs to the wide $AA'_3B_4O_{12}$ perovskite family phase, where A is generally a large monovalent or divalent or rare-earth cation; A′ stands for Cu^{2+} or Mn^{3+}; and B can be $Mn^{4+/3+}$, Ti^{4+}, Ru^{4+}, or Ge^{4+} [7, 8]. In all these compounds, the crystal symmetry is cubic (space group $Im\bar{3}$) with a doubling of the ideal ABO_3 perovskite cell. The superstructure is due to the ordering of the A and A′ ions and the distortion of the oxygen sublattice, which leads to a three-dimensional network of strongly tilted BO_6 octahedra sharing corners [9]. The B–O–B angle is ∼142° instead of 180°, as in the ideal perovskite structure. This distortion creates two different polyhedra at the A/A′ site: a slightly distorted 12 oxygen-coordinated A site and a grossly distorted icosahedron at the A′ site. There are three sets of A′–O distances at ∼1.9, 2.8 and 3.2 Å, each forming an approximately square-planar coordination for A′ cations [9]. One of the unusual characteristics of this structure is that it requires a Jahn–Teller distorted ion, such as Cu^{2+}, at the A′ site. Cu^{2+} can be partially or completely substituted by Mn^{3+} (d^4, also a Jahn–Teller ion) in the $CaCu_{3-x}Mn_{4+x}O_{12}$ system [6, 10].

The recent interest in this family of compounds was triggered by the description of CMR properties in the series $CaCu_{3-x}Mn_{4+x}O_{12}$, prepared under 180 bar of oxygen pressure and moderate temperatures of 700 °C [11]. A related compound, with stoichiometry $Na_{0.5}Ca_{0.5}Cu_{2.5}Mn_{4.5}O_{12}$, was also reported to show similar magnetotransport properties to $CaCu_{2.5}Mn_{4.5}O_{12}$ [12]. $CaCu_{2.5}Mn_{4.5}O_{12}$ has been prepared at moderate pressures of 2 GPa, in sealed gold capsules containing $KClO_4$ as oxidizing agent [5]. In this paper we describe the preparation, under moderate pressure conditions, of a new series of perovskites of nominal stoichiometry $CaCu_3(Mn_{4-x}Fe_x)O_{12}$ ($0 \leqslant x \leqslant 1$). Our primary aim was to improve the magnetic properties of the parent perovskite $CaCu_3Mn_4O_{12}$ by the introduction of Fe cations at the Mn sublattice. We report on the structural and crystallochemical characterization of these complex perovskites by neutron powder diffraction techniques, especially sensitive to the replacement of Mn by Fe given the opposite scattering lengths of both elements, complemented with a Mössbauer spectroscopy study for the $x = 1.0$ sample. The magnetic and magnetotransport properties of these new materials are described and discussed.

2. Experimental details

Materials of nominal stoichiometry $CaCu_3(Mn_{4-x}Fe_x)O_{12}$ ($x = 0$, 0.5 and 1) were obtained as black polycrystalline powders by a citrate technique from stoichiometric amounts of analytical grade $CaCO_3$, $Cu(NO_3)_2{\cdot}3H_2O$, $FeC_2O_4{\cdot}2H_2O$ and $MnCO_4$. The high-pressure preparation (2 GPa, 1000 °C) is described in detail elsewhere [6]. A fraction of the raw products, obtained as dense, homogeneous pellets, was partially ground to perform the structural, magnetic and Mössbauer characterization; some as-grown pellets were kept for magnetotransport measurements.

Table 1. Unit-cell parameters and magnetic constants for $CaCu_3(Mn_{4-x}Fe_x)O_{12}$. The $x = 0$ data are taken from [5]. Unit-cell parameters for $x = 0$ and 1.0 were determined from NPD data, and for $x = 0.5$ from XRD data.

x	a (Å)	T_C (K)	M_s (μ_B/fu)	μ_{eff} (μ_B/fu)	θ_{Weiss} (K)	MR (300 K, 9 T) (%)
0	7.2279(1)	345	10.5	6.73	282	7
0.5	7.2519(1)	275	10.6	8.00	290	6.5
1.0	7.267 93(7)	235	9.8	8.36	251	4.5

The reaction products were characterized by x-ray diffraction (XRD) for phase identification and to assess phase purity. A neutron powder diffraction (NPD) pattern of $CaCu_3(Mn_3Fe)O_{12}$ was collected using the high-resolution HRPT diffractometer of the SINQ spallation source, at the Paul Scherrer Institute, Villigen, Switzerland. The sample, weighing 0.8 g, was packed in a cylindrical vanadium holder of 6 mm diameter. A room-temperature (RT) pattern was collected with a wavelength of 1.494 Å and a counting time of 4 h.

The NPD patterns were analyzed by the Rietveld method, using the FullProf program [13]. The line shape of the diffraction peaks was generated by a pseudo-Voigt function, and the background refined to a fifth-degree polynomial. The coherent scattering lengths for Ca, Cu, Mn, Fe and O were, respectively, 4.70, 7.718, −3.73, 9.45, 5.803 fm. In the final run the following parameters were refined: background coefficients, zero-point, half-width, pseudo-Voigt and asymmetry parameters for the peak shape, scale factor, positional, mixed occupancy factors for Fe/Mn, thermal isotropic factors for all the atoms and unit-cell parameters.

The sample for Mössbauer spectroscopy study was prepared as follows. The powder material, $CaCu_3(Mn_3Fe)O_{12}$, was mixed with polyvinyl alcohol powder (glue substance) and then was pressed into a disc with diameter 12 mm. The thickness of the disc was chosen to have 7 mg cm^{-2} Fe. The Mössbauer spectrum was taken at RT in the transmission mode with a conventional constant acceleration spectrometer. A ^{57}Co(Rh) source with activity of 20 mCi was used. The spectrum was fitted using an integral Lorentzian line shape approximation [14, 15]. This approach permits us to separate the absorber line widths and to avoid the saturation thickness effect. The isomer shifts are referred to the centroid of an α-Fe foil reference spectrum at RT. The geometric effect due to the source motion is taken into account as well.

The dc magnetic susceptibility was measured with a commercial SQUID magnetometer on powdered samples, in the temperature range 2–400 K; transport and magnetotransport measurements were performed by the conventional four-probe technique, under magnetic fields up to 9 T in a PPMS system from Quantum Design.

3. Results and discussion

3.1. Structural refinement

The products were obtained as black, well-crystallized powders. The XRD patterns are characteristic of cubic perovskites showing sharp, well-defined superstructure reflections due to the 1:3 ordering of Ca and Cu cations. Table 1 includes the unit-cell parameters for all the samples. The data for $x = 0$ (Fe-undoped compound) correspond to $CaCu_{2.5}Mn_{4.5}O_{12}$, containing 0.5 Mn^{3+} at the Cu^{2+} sublattice [5], since the parent $CaCu_3Mn_4O_{12}$ material cannot be accessed under the moderate pressure conditions utilized in this work. The crystal structure refinement of the sample $CaCu_3Mn_3FeO_{12}$ was performed from high-resolution NPD data collected at RT with a wavelength $\lambda = 1.494$ Å. The structure was refined in the $Im\overline{3}$ (No. 204)

Table 2. Unit-cell, positional, thermal parameters and site occupancies for $CaCu_3Mn_3FeO_{12}$, refined in the cubic $Im\bar{3}$ (No. 204) space group, $Z = 2$, $a = 7.267\,93(7)$ Å, from NPD data at 295 K. Reliability factors: $\chi^2 = 15.5$; $R_p(\%) = 3.02$; $R_{wp}(\%) = 4.22$; $R_I(\%) = 3.35$.

Atom	Site	x	y	z	B (Å^2)	f_{occ}
Ca	2*a*	0	0	0	0.35(6)	1.0
Cu	6*b*	0	1/2	1/2	0.65(4)	0.726(3)
Mn_A	6*b*	0	1/2	1/2	0.65(4)	0.241(3)
Fe_A	6*b*	0	1/2	1/2	0.65(4)	0.033
Mn_B	8*c*	1/4	1/4	1/4	0.23(12)	0.795(3)
Fe_B	8*c*	1/4	1/4	1/4	0.23(12)	0.205(3)
O	24*g*	0	0.3044(1)	0.1813(1)	0.57(2)	1.0

space group, with unit-cell parameters related to $\mathbf{a}_0$ (ideal cubic perovskite, $\mathbf{a}_0 \approx 3.8$ Å) as $\mathbf{a} \approx 2\mathbf{a}_0$, using the $CaCu_3Mn_4O_{12}$ structure as the starting model, with Ca atoms at 2*a* (0 0 0) positions, Cu at 6*b* (0 1/2 1/2) positions, Mn at 8*c* (1/4 1/4 1/4), and O at 24*g* (x y 0) sites. A rough fit of the data was obtained for this starting model ($R_I \approx 15\%$). As a second step, Fe atoms were introduced at random at 8*c* positions together with Mn, and the complementary occupancy factors were refined, constrained to a full occupancy, notably improving the quality of the fit. Finally, the possibility of partial occupancy of 6*b* positions by some Mn cations was also checked and this also led to a drop of the discrepancy factors. The crystallographic formula after this refinement was $Ca[Cu_{2.29(1)}Mn_{0.71(1)}]_{6b}[Mn_{3.18(1)}Fe_{0.82(1)}]_{8c}O_{12}$.

As will be described below, a Mössbauer study on the same sample suggested that, besides the major Fe content found at octahedral positions, 11% of Fe atoms are found at the square-planar sites together with Cu. In the present NPD study the presence of some Fe atoms at this site could not be confirmed since the 6*b* sites are simultaneously occupied by Cu (with positive scattering length, $b = 7.718$ fm) and Mn atoms (with negative scattering length, $b = -3.73$ fm), in such a way that the occupancy factor of a third atom, Fe (with positive $b = 9.45$ fm), cannot be determined. In a further refinement taking into account the information obtained from the Mössbauer study, we considered a structural model containing a fixed amount of 11% Fe at 6*b* positions, then refining the occupancy of Cu versus Mn, constrained to full occupancy. The crystallographic formula of the main phase after the final refinement is $Ca[Cu_{2.18(1)}Mn_{0.72(1)}Fe_{0.10}]_{6b}[Mn_{3.18(1)}Fe_{0.82(1)}]_{8c}O_{12}$, completely compatible with the Mössbauer results, as we will describe below.

Two minor impurity phases were identified as $K_{1.33}Mn_8O_{16}$ with hollandite structure (coming from partial reaction of $KClO_4$ with MnO_2) and C (graphite from the heater); both phases were introduced in the refinement, obtaining from the scale factors a relative amount in weight of 7.50% of hollandite and 1.65% of C. An excellent fit was obtained, as illustrated in figure 1. Table 2 lists the refined structural and thermal parameters; table 3 contains the mean interatomic distances and some selected bond angles. We should highlight that (Mn, Fe)–O distances within the $(Mn, Fe)O_6$ octahedra (1.9255(8) Å) are significantly longer than those observed in $CaCu_{2.5}Mn_{4.5}O_{12}$, of 1.915(1) Å [5], which is consistent with the incorporation of larger Fe^{3+} (ri = 0.645 Å) [16] cations in the Mn^{4+} (0.53 Å) sublattice.

A view of the crystal structure of $CaCu_3(Mn_3Fe)O_{12}$ is given in figure 2. The perovskite structure is fairly distorted due to the small size of Ca^{2+} and (Cu^{2+}, Mn^{3+}) cations, which force the $(Mn, Fe)O_6$ octahedra to tilt in order to optimize the Ca–O bond distances. The tilting angle of the octahedra can be simply derived from the Mn–O–Mn angle, found to be 19° at RT. The main result of the neutron study is that the Fe cations are located at the B positions of the perovskite, together with Mn at 8*c* sites. It is also remarkable that there is

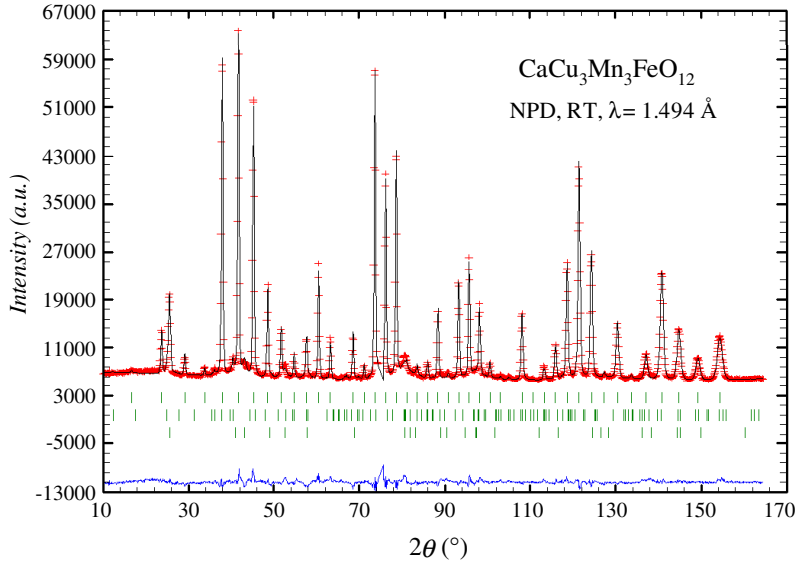

Figure 1. Observed (crosses), calculated (full line) and difference (bottom) NPD Rietveld profiles for $CaCu_3Mn_3FeO_{12}$ at RT. The three series of tick marks correspond to the allowed Bragg reflections for the main phase, an impurity with hollandite structure ($K_{1.33}Mn_8O_{16}$) and C (graphite).

Table 3. Main bond distances (Å) and selected angles (°) for $CaCu_3Mn_3FeO_{12}$ determined from NPD data at 295 K.

CaO_{12} polyhedra	
Ca– O (*x*12)	2.5745(8)
(Cu, Mn)O_{12} polyhedra	
Cu– O (*x*4)	1.939(1)
Cu– O (*x*4)	2.719(1)
Cu– O (*x*4)	3.203(1)
O–Cu–O[a]	94.39(8)
(Mn, Fe)O_6 octahedra	
Mn– O (*x*6)	1.9255(9)
O–Mn–O	90.10(6)
Cu–O–Mn	109.07(3)
Mn–O–Mn	141.37(2)

[a] for short Cu–O distances, within CuO_4 square units.

incorporation of a significant amount of Mn^{3+} at the Cu^{2+} positions, as happens in the $x = 0$ compound, containing 0.5 Mn^{3+} at the Cu^{2+} sublattice [5]; it seems that the presence of Mn^{3+} helps the stabilization of these materials under moderate pressure (2 GPa) conditions. For the mentioned crystallographic formula, assuming oxidation states of 2+ for Ca and Cu, 3+ for Mn at Cu positions and 3+ for Fe at octahedral and square-planar positions (as demonstrated in the Mössbauer study), it results that the valence for Mn at B positions is exactly 4.00+. The presence of some oxygen vacancies is not excluded, although this could not be checked from the neutron data: the refinement became unstable when varying the O occupancy factors, showing large correlations with the mixed occupancy at A′ and B positions.

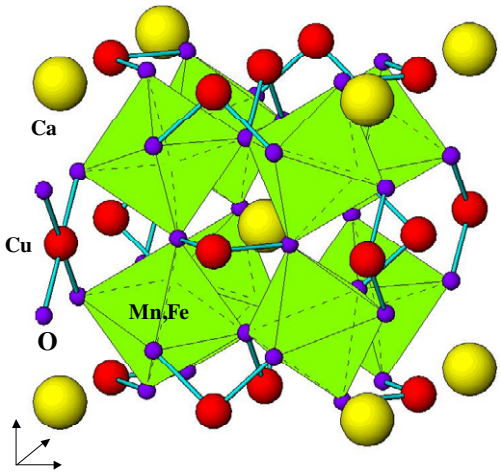

Figure 2. Schematic representation of the crystal structure of $CaCu_3Mn_4O_{12}$ and derivatives, highlighting the considerable tilting of the MnO_6 octahedra, and the square-planar coordination of Cu^{2+} cations.

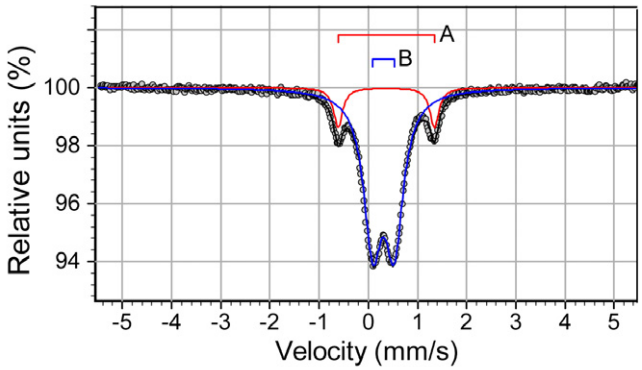

Figure 3. Mössbauer spectra for $CaCu_3Mn_3FeO_{12}$ at RT.

Table 4. Mössbauer parameters obtained from the fit of the spectra of figure 3.

Quadrupole doublets	IS (mm s^{-1})	QS (mm s^{-1})	FWHM (mm s^{-1})	Relative area %
Doublet A	0.423 ± 0.003	1.92 ± 0.006	0.12 ± 0.01	10.9 ± 0.4
Doublet B	0.369 ± 0.002	0.42 ± 0.002	0.33 ± 0.01	89.1 ± 0.5

3.2. Mössbauer spectroscopy study

The measured spectrum corresponding to $CaCu_3(Mn_3Fe)O_{12}$ at RT is shown in figure 3. The parameters of the fitted components of the spectrum corresponding to isomer shift (IS), quadrupole splitting (QS), full width at half maximum (FWHM) of the absorption resonance lines, and relative spectral area are shown in table 4. The spectrum was fitted by superposition of two quadrupole doublets. The isomer shifts of the doublet A and doublet B are 0.423 and 0.369 mm s^{-1} respectively. The quadrupole splitting for doublets A and B is quite different: 1.92 mm s^{-1} and 0.42 mm s^{-1} respectively.

The isomer shift, δ, is an important Mössbauer parameter since it is closely related to the valence and coordination number (CN). The shift of the peak position is observed as a result of the Coulombic interaction between the nucleus and electrons. The change of the s-electron density at the nuclear site is reflected in δ. In the case of ^{57}Fe an increase in the s-electron density in the absorber is observed as a decrease in δ. For oxides where iron is in high-spin state there is a good correlation between the isomer shift of Mössbauer spectrum and the valence state. According to systematic data of Greenwood and Gibb [17], Dyar and Schaefer [18], and Dyar *et al* [19], both quadrupole doublets should be attributed to Fe^{3+}.

We shall recall that the quadrupole splitting (QS) corresponds to the peak separation and it is equivalent to the gap of two energy levels in the excited state of iron nuclei. The splitting of energy levels into two degenerate levels is due to the electric field gradient (EFG) at the nuclear site produced by the electrons and/or neighboring atoms. Thus, QS originates from the nuclear quadrupole interaction between the nucleus with a nuclear spin, I, and EFG, which is the second derivative of the electrostatic potential.

In the case of the Fe-doped compounds studied, neutron diffraction refinements clearly indicate that iron is occupying predominantly the octahedral positions partially replacing manganese. We attribute the doublet B to 89% of the total Fe^{3+} occupying octahedral positions, where it replaces Mn: in this case the distortion of the corresponding octahedron is comparatively small (QS $=$ 0.42 mm s^{-1}). Nevertheless, some part of it could be in the square-planar positions instead of Cu. If we attribute doublet A to Fe^{3+} in square-planar positions, partially replacing Cu^{2+}, the electric field gradient should be relatively strong and, correspondingly, the quadrupole splitting should be considerably high: for doublet A, QS $=$ 1.92 mm s^{-1}. Moreover, Tretyakov and Goodilin [20] found for Fe^{3+} placed at the square-planar units of Cu^{2+} in Fe-doped superconducting materials of the family $YBa_2Cu_3O_{7-d}$ QS values around 1.8–2 mm s^{-1}, as observed in the present work. There is only 11% of the total Fe occupying these very distorted positions.

It should be mentioned that the resonance lines of doublet B are broadened about three times of the natural line widths, while doublet A does not show any broadening (see the FWHM in table 4). The broadening of doublet B could be explained by random distribution of Fe^{3+} at octahedral positions instead of Mn. That random distribution of the so-called next-nearest neighbors (after the first oxygen surrounding) leads to the broadening of doublet B. In contrast, despite the random distribution of Fe^{3+} in the A sites, the resonance lines of that doublet are not broadened. The reason for this is twofold: first, the iron replacing Cu in the Cu sublattice is of relatively small percentage (see the relative spectral area in table 1); secondly, the distance Cu–Cu is greater than the distance Mn–Mn.

3.3. Magnetic properties

The magnetization versus temperature data (figure 4) show in all cases a saturation characteristic of the spontaneous ferromagnetic ordering described earlier [2] for the parent perovskite $CaCu_3Mn_4O_{12}$. The magnetic parameters are summarized in table 1. The Fe-undoped compound, $CaCu_{2.5}Mn_{4.5}O_{12}$, exhibits a T_C (given by the inflexion in the magnetization) at 345 K, slightly lower than the reported Curie temperature for the parent $CaCu_3Mn_4O_{12}$ oxide, of 355 K [2]. In the Fe-substituted samples, a progressive reduction in T_C is displayed: T_C values of 275 and 235 K are observed for $CaCu_3(Mn_{4-x}Fe_x)O_{12}$ with nominal x values of 0.5 and 1.0, respectively. The magnetization versus magnetic field isotherms (figure 5) also correspond to ferromagnetic materials, with a sharp saturation for fields smaller that 1 T. The sample with Fe content $x = 1.0$ exhibits a significant decrease of the saturation magnetization (M_s), which suggests the appearance of antiferromagnetic interactions between

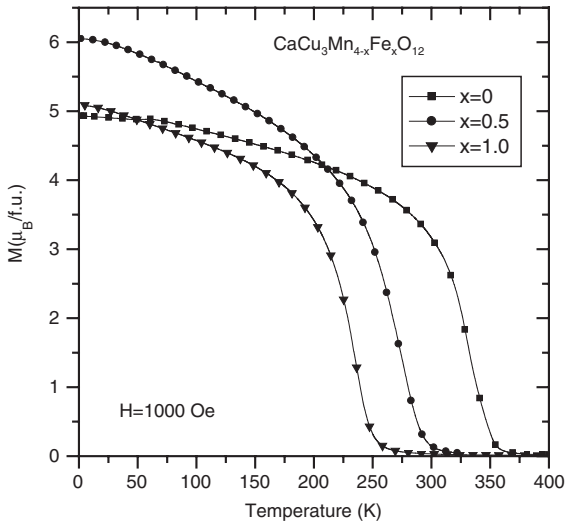

Figure 4. Temperature dependence of the magnetization for $CaCu_3Mn_{4-x}Fe_xO_{12}$ ($x = 0, 0.5, 1.0$).

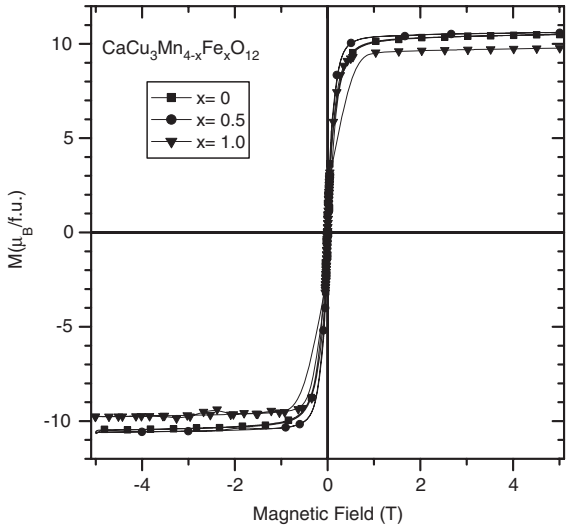

Figure 5. Magnetization versus magnetic field isotherms for $CaCu_3Mn_{4-x}Fe_xO_{12}$ ($x = 0$, 0.5, 1.0).

the Fe^{3+} ($S = 5/2$) and Mn^{4+} ($S = 2$) spins, which diminish the global magnetization. In the parent material, the global magnetization results from the opposite alignment of the copper and manganese magnetic moments. The positive Weiss temperatures (θ_{Weiss}) found along the series (table 1) suggest that the predominant interactions are the ferromagnetic superexchange coupling within the Mn and Cu sublattices, that are then antiferromagnetically coupled. The observed decrease of T_C (figure 4), saturation magnetization (figure 5) and Weiss constants (table 1) strongly support the hypothesis that Mn and Fe spins at B sites are antiferromagnetically coupled, reducing the average ordered magnetic moment corresponding to the B sublattice.

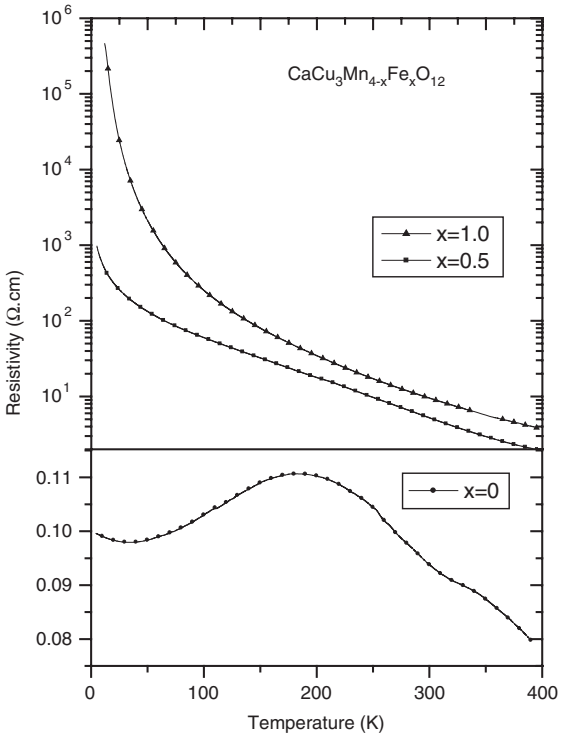

Figure 6. Resistivity versus temperature for $CaCu_3Mn_{4-x}Fe_xO_{12}$ ($x = 0.5, 1.0$). The lower panel corresponds to $x = 0$, taken from [5].

3.4. Magnetotransport properties

The $CaCu_3(Mn_{4-x}Fe_x)O_{12}$ samples display a semiconducting behavior in all the temperature range (0–400 K), as observed in the upper panel of figure 6; they show an RT resistivity of about 10 Ω cm, whereas the Fe-undoped sample ($CaCu_{2.5}Mn_{4.5}O_{12}$, lower panel of figure 5) shows a semiconductor-to-metal transition around 180 K and exhibits a considerable lower RT resistivity of 0.093 Ω cm (taken from [5]). The low resistivity value of the parent $Ca(Cu_{2.5}Mn_{0.5})_A(Mn_4)_BO_{12}$ oxide is due to the mixed valence state induced on the Mn cations at B positions: assuming a divalent oxidation state for Ca and Cu and trivalent for Mn at A positions (as demonstrated in a recent spectroscopic study [6]), the octahedral Mn cations exhibit an average valence of 3.875+. The huge increase in resistivity in the Fe-doped samples can be accounted for as follows: the introduction of Fe^{3+} at B positions substantially suppresses the Mn^{3+}–Mn^{4+} mixed valence state at the octahedral sites; for instance $Ca[Cu_{2.18(1)}Mn_{0.72(1)}Fe_{0.10}]_A[Mn_{3.18(1)}Fe_{0.82(1)}]_BO_{12}$ exhibits a net valence of 4.00+ for Mn_B cations, thus hindering the hopping mechanism between adjacent Mn^{3+} and Mn^{4+} which is responsible for the charge transport in the Fe-undoped sample. We assume that the charge transfer between neighboring Fe^{3+} and Mn^{4+} is negligible, given the energy mismatch between Fe and Mn $3e_g$ orbitals.

Regarding the changes in $R(T)$ under a magnetic field we define $MR(H) = 100 \times [R(H) - R(0)]/R(0)$ as the magnetoresistive response. Figure 7 illustrates the magnetoresistance isotherms for $CaCu_3(Mn_3Fe)O_{12}$. The magnetoresistance is negative and reaches a maximum value of −14% at 50 K and 9 T. The MR is still significant at RT, displaying

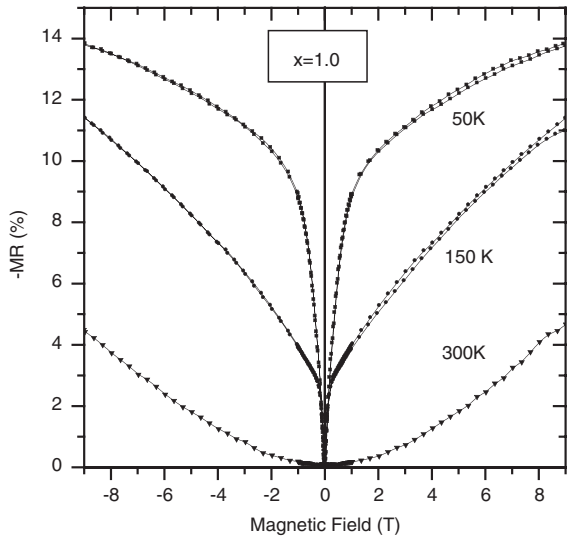

Figure 7. MR versus magnetic field isotherms for $CaCu_3Mn_3FeO_{12}$.

values close to -4.5% for $H = 9$ T. Unlike the parent compound, which shows a strong component of low-field MR (defined for magnetic fields lower than 1 T), this material exhibits a concave MR curve at 300 K, since T_C is much lower (235 K) than RT. By contrast, the low-field component is not negligible (about 3%) at 150 K, for external applied fields as low as 0.25 T. This low-field response is remarkably narrow and could be related to the decrease in the number of charge carriers in this material. Recently, Majumdar and Littlewood [21] described a reciprocal relationship between the MR and the number of charge carriers, in such a way that a decrease in the carriers density is concomitant with an increase in MR. In the case of $CaCu_3Mn_4O_{12}$ and $CaCu_3(Mn_3Fe)O_{12}$, where the MR is not coupled with T_C, there is an important proportion of extrinsic MR, that is generated at the grain boundaries or magnetic-domain walls, where the misorientation of the magnetic moments is more easily suppressed by the application of low magnetic fields. The extrinsic low-field MR can be increased in magnitude by reducing the number of carriers, in such a way that the contribution of the grain boundaries or magnetic-domain walls to the total electrical resistance becomes important. The chemical replacement of Mn by Fe leads to an effective hole-injection effect involving a dramatic increase of the bulk resistivity and a relative improvement of the extrinsic MR, due to the enhancement of the grain-boundary or domain-wall contribution to the electrical resistance.

4. Conclusions

New phases of stoichiometry $Ca^{2+}(Cu^{2+}_{3-y-z}Mn^{3+}_{y}Fe^{3+}_{z})_A(Mn^{4+}_{4-x}Fe^{3+}_{x})_BO_{12}$ with a perovskite-related structure have been synthesized at moderate pressures (2 GPa) in the presence of an oxidizing agent. The structural refinement from high-resolution NPD data allowed us to unravel the crystallographic features in the $x = 1$ sample. Owing to the contrast between the neutron scattering lengths of Mn and Fe, we could discern that Fe cations occupy the B octahedral positions of the complex ABO_3 perovskite, and a part of Mn, adopting a trivalent oxidation state, is placed at the A positions together with Cu^{2+} cations. The occupancy of Fe^{3+} at the B positions is confirmed by Mössbauer spectroscopy for the $x = 1$ compound. This technique also suggests that 11% of the total Fe^{3+} cations are placed at the square-planar

positions together with Cu^{2+} and Mn^{3+}. Magnetization measurements suggest the presence of antiferromagnetic Fe–O–Mn interactions, hence decreasing T_C, M_s and θ_{Weiss}. The resistivity of the Fe-doped samples is semiconducting-like and presents a much higher magnitude than that of the undoped compound: the introduction of Fe^{3+} at the octahedral sublattice suppresses the mixed-valence state over the Mn_B positions, thus drastically decreasing the charge carrier concentration. Given that $T_C = 235$ K for $CaCu_3(Mn_3Fe)O_{12}$, its MR at 300 K is inferior to that of the undoped compound, but at 150 K a sharp low-field component is observed.

Acknowledgments

Financial support from CICyT, Spain, under the Projects MAT2004-0479 is acknowledged. This work was partially performed at the spallation source SINQ, Paul Scherrer Institute, Villigen, Switzerland. We acknowledge financial support from a CSIC-BAS cooperation Project CSIC2005BG0012. KK, IS and TR thank the Bulgarian NSF for funding the Project #F-1012.

References

[1] Ramirez A P 1997 *J. Phys.: Condens. Matter* **9** 8171
[2] Zeng Z, Greenblatt M, Subramanian M A and Croft M 1999 *Phys. Rev. Lett.* **82** 3164
[3] Wu H, Zheng Q and Gong X 2000 *Phys. Rev.* B **61** 5217
[4] Weth R and Pickett W E 2001 *Phys. Rev.* B **65** 14415
[5] Sánchez-Benítez J, Alonso J A, Martínez-Lope M J, Casais M T, Martínez J L, de Andrés A and Fernández-Díaz M T 2003 *Chem. Mater.* **15** 2193
[6] Sánchez-Benítez J, Prieto C, de Andrés A, Alonso J A, Martínez-Lope M J and Casais M T 2004 *Phys. Rev.* B **70** 24419
[7] Chenavas J, Joubert J C, Marezio M and Bochu B 1975 *J. Solid State Chem.* **14** 25
[8] Bochu B, Joubert J C, Collomb A, Ferrand B and Samaras D 1980 *J. Magn. Magn. Mater.* **15** 1319
[9] Deschizeaux M N, Joubert J C, Vegas A, Collomb A, Chenavas J and Marezio M 1976 *J. Solid State Chem.* **19** 45
[10] Sánchez-Benítez J, Alonso J A, de Andrés A, Martínez-Lope M J, Casais M T and Martínez J L 2004 *J. Magn. Magn. Mater.* **272–276** e1407
[11] Zeng Z, Greenblatt M, Sunstrom J E, Croft M and Khalid S 1999 *J. Solid State Chem.* **147** 185
[12] Zeng Z, Greenblatt M and Croft M 1998 *Phys. Rev.* B **58** R595
[13] Rodríguez-Carvajal J 1993 *Physica* B **192** 55
[14] Shenoy G K, Friedt J M, Maleta H and Ruby S L 1974 *Mössbauer Eff. Methodol.* **9** 277
[15] Cranshaw T E 1974 *J. Phys. E: Sci. Instrum.* **7** 122
[16] Shannon R D 1976 *Acta Crystallogr.* A **32** 751
[17] Greenwood N N and Gibb T C 1971 *Mössbauer Spectroscopy* (London: Chapman and Hall) p 91
[18] Dyar M and Schaefer M 2004 *Earth Planet. Sci. Lett.* **218** 243
[19] Dyar M, Agresti D, Schaefer M, Grant C and Sklute E 2006 *Annu. Rev. Earth Planet. Sci.* **34** 83
[20] Tretyakov Y D and Goodilin E A 2004 *Pure Appl. Chem.* **76** 1749
[21] Majumdar P and Littlewood P B 1998 *Nature* **395** 479